Plasma membrane phosphoinositide balance regulates cell shape during *Drosophila* embryo morphogenesis

Alessandra Reversi, Eva Loeser, Devaraj Subramanian, Carsten Schultz, and Stefano De Renzis

European Molecular Biology Laboratory (EMBL) Heidelberg, 69117 Heidelberg, Germany

Remodeling of cell shape during morphogenesis is driven by the coordinated expansion and contraction of specific plasma membrane domains. Loss of this coordination results in abnormal cell shape and embryonic lethality. Here, we show that plasma membrane lipid composition plays a key role in coordinating plasma membrane contraction during expansion. We found that an increase in PI(4,5)P_2 levels caused premature actomyosin contraction, resulting in the formation of shortened cells. Conversely, acute depletion of PI(4,5)P_2 blocked plasma membrane expansion and led to premature actomyosin disassembly. PI(4,5)P_2-mediated contractility is counteracted by PI(3,4,5)P_3 and the zygotic gene *bottleneck*, which acts by limiting myosin recruitment during plasma membrane expansion. Collectively, these data support a model in which the ratio of PI(4,5)P_2/PI(3,4,5)P_3 coordinates actomyosin contractility and plasma membrane expansion during tissue morphogenesis, thus ensuring proper cell shape.

Introduction

Cell shape changes are of fundamental importance during embryonic development. Localized changes in cell shape, such as apical constriction and basal expansion, drive folding of epithelial tissues whereas more complex shape changes bring about specialized function in terminally differentiated cells (Glotzer, 2005; Fernandez-Gonzalez et al., 2009; Martin et al., 2009; Pollard, 2010; Rauzi et al., 2010; Salbreux et al., 2012). Morphological remodeling depends on tightly coordinated cycles of plasma membrane expansion and contraction (Lecuit and Pilot, 2003; Fabrowski et al., 2013; Figard et al., 2013). Whereas plasma membrane expansion requires the addition of new membranes, plasma membrane contraction depends primarily on forces generated by the actomyosin apparatus (Behrndt et al., 2012; Mason et al., 2013). To achieve effective cell shape changes, actomyosin contraction must be kept on hold during plasma membrane expansion. The mechanisms underlying this temporal coordination are poorly understood.

The cellularization of the early *Drosophila melanogaster* embryo provides a suitable model system to address the mechanisms underlying coupling of actomyosin contraction with plasma membrane expansion during tissue morphogenesis (Schejter and Wieschaus, 1993b; Sullivan and Theurkauf, 1995). The early embryo undergoes 13 rapid nuclear divisions without intervening cytokinesis. During interphase of cycle 14, cellularization transforms the syncytial embryo into a monolayer of 6,000 columnar epithelial cells. This morphogenetic process starts with the invagination of plasma membrane in between cortically anchored nuclei, followed by expansion for ∼40 µm perpendicular to the cortex of the embryo. This invagination process increases the surface area ∼30-fold and is characterized by a slow (40 min) and a fast phase (20 min) of membrane growth (Lecuit and Wieschaus, 2000). The slow phase begins with the invagination of the plasma membrane and assembly of cleavage furrows, which establish a network of interconnected hexagonal actomyosin arrays at their leading edge (Schejter and Wieschaus, 1993a). The contractile properties and molecular composition of this network change over time with the level of myosin-II increasing progressively (Royou et al., 2004; Thomas and Wieschaus, 2004). As the invaginating plasma membrane reaches the base of the nuclei, the hexagonal network is converted into individual actomyosin rings, which eventually contract and drive the closure of the cells basally. This temporal sequence of events is under the regulation of zygotic transcription (Merrill et al., 1988; Wieschaus and Sweeton, 1988).

Correspondence to Stefano De Renzis: derenzis@embl.de

Abbreviations used in this paper: 5Ptase, 5-phosphatase; AM, acetoxymethyl; Bnk, Bottleneck; PI3-kinase, phosphatidylinositol 3-kinase; *sqh*, *spaghetti squash*.

The Rockefeller University Press $30.00
J. Cell Biol. Vol. 205 No. 3 395–408
www.jcb.org/cgi/doi/10.1083/jcb.201309079

Previous zygotic screens led to the identification of the *bottleneck* mutant phenotype, whose major characteristic is the premature contraction of the actomyosin network (Schejter and Wieschaus, 1993a). As a consequence, nuclei remain trapped in hyper-constricted actomyosin rings and are pushed away from the epithelium, resulting in the formation of short cells without nuclei. Bottleneck (Bnk) is zygotically expressed, localizes to the hexagonal actomyosin arrays during the slow phase, and is then quickly degraded during the fast phase when the plasma membrane reaches the base of the nuclei and the network breaks down into individual contractile actomyosin rings. In *bottleneck* mutant embryos the transition into contractile actomyosin rings occurs during the slow phase, causing the characteristic morphological alterations described above (Schejter and Wieschaus, 1993a; Theurkauf, 1994). Bottleneck is a highly basic protein of ∼300 residues without any known protein domain or interacting factor, which could help explain its mechanism of action.

Plasma membrane phosphoinositides, in particular $PI(4,5)P_2$ and $PI(3,4,5)P_3$, play an important role in coupling actin with membrane dynamics (Insall and Weiner, 2001; Janetopoulos and Devreotes, 2006; Comer and Parent, 2007). Many actin-binding proteins are recruited to $PI(4,5)P_2$- or $PI(3,4,5)P_3$-enriched plasma membrane domains, where they control the rate of actin polymerization (Mayer et al., 1993; McLaughlin et al., 2002; Moss, 2012). Altering $PI(4,5)P_2$ and $PI(3,4,5)P_3$ levels might therefore provide insight into the mechanisms underlying the temporal coordination between plasma membrane remodeling and contractility during morphogenesis. However, the relatively long time that is required to manipulate phosphoinositide levels using traditional genetic approaches, such as knock-out or overexpression of enzymes controlling their metabolism, has made it so far difficult to characterize their impact on morphogenesis (Schultz, 2010). Furthermore, phosphoinositides are likely required at multiple stages during development, thus preventing interference with their function at specific developmental stages without affecting earlier processes. To circumvent this limitation, we used a combination of membrane-permeant phosphoinositides and the rapamycin-inducible protein dimerization system to temporally control the levels of phosphoinositides during cellularization. Using this approach we demonstrate that $PI(4,5)P_2$ is required for the assembly of the actomyosin network and for promoting its contractility during the fast phase. $PI(3,4,5)P_3$ is required for maintaining the structural organization of the actomyosin network into an integrated array of hexagonal units, thus preventing constriction of actomyosin rings during the slow phase. We further demonstrate that $PI(3,4,5)P_3$ is required to stabilize Bnk at the furrows and that Bnk acts by stabilizing actin filaments and by inhibiting myosin recruitment during the slow phase of cellularization. This $PI(4,5)P_2$/$PI(3,4,5)P_3$-based mechanism ensures that cells of the correct size and shape are generated.

Results

Increasing $PI(4,5)P_2$ levels during cellularization causes premature contraction of the actomyosin network

To investigate the role of plasma membrane phosphoinositides during cellularization without interfering with earlier $PI(4,5)P_2$/$PI(3,4,5)P_3$-dependent developmental processes, we tested the effect of an acute administration of $PI(4,5)P_2$ and $PI(3,4,5)P_3$. We used membrane-permeant analogues henceforth referred to as $PI(4,5)P_2$/AM and $PI(3,4,5)P_3$/AM. These compounds are modified by the addition of acetoxymethyl esters (AM esters) and butyrates, which mask the charged phosphate groups and the hydroxyl groups, respectively. The cytoplasmic cleavage of these bioactivatable esters leads to unmasking of phosphate groups and a resulting reconstitution of biological function. Importantly, the masked compounds lack the tendency of forming insoluble precipitates with divalent cations and are therefore applicable in physiological buffer systems (Schultz, 2003; Laketa et al., 2009).

We investigated the effect of $PI(4,5)P_2$/AM and $PI(3,4,5)P_3$/AM on morphogenesis in embryos expressing the regulatory light chain of nonmuscle myosin-II (*spaghetti squash* [*sqh*]) tagged with GFP (Sqh::GFP), which allows visualization of myosin network dynamics (Royou et al., 2004). Additionally, embryos expressing Spider::GFP (Morin et al., 2001) and histone::GFP were used to visualize the plasma membrane and the nuclei, respectively (see Fig. 1, A and B for a schematic of cellularization). Pre-cellularizing embryos were injected with either $PI(4,5)P_2$/AM or $PI(3,4,5)P_3$/AM and imaged using two-photon microscopy. In control-injected embryos, cellularization proceeded without any visible morphological abnormalities (Fig. 1, C–C″; see also Fig. 2, A and B; and Video 1). Injection of $PI(4,5)P_2$/AM resulted in a strong and reproducible phenotype characterized by premature constriction of actomyosin rings and shortening of the cells (Fig. 1, D–D″; and Video 2). Imaging of Sqh::GFP showed that the normal hexagonal pattern of interconnected actomyosin arrays did not form. Instead, actomyosin rings constricted during the slow phase before the plasma membrane had passed the base of the nuclei (Fig. 1 D″). As a consequence, the nuclei remained trapped in constricted actomyosin rings and were pushed toward the interior of the embryo (Fig. 2 A′), resulting in the formation of short cells with abnormal shape (Fig. 2 B′). Imaging from an apical cross section demonstrated that although the furrows had invaginated for only 5 µm, the area of most actomyosin rings was strongly reduced (Fig. 1 G) compared with control-injected embryos (Fig. 1 F), indicating that the actomyosin network was hyper-contracted. Injection of $PI(4,5)P_2$/AM before cycle 13 did not alter the normal dynamics of metaphase furrow formation and regression, thus showing that the $PI(4,5)P_2$-induced phenotype is specific for the early phase of cellularization. Only when embryos entered cycle 14 did the hyper-constricted phenotype manifest itself (Fig. S1, A–D). We confirmed that ectopic $PI(4,5)P_2$/AM was indeed incorporated into the plasma membrane by showing increased recruitment of PLCδ1-PH-GFP, a well-established $PI(4,5)P_2$ sensor (Fig. S1, E and F).

$PI(3,4,5)P_3$ is also localized at the plasma membrane and regulates membrane/cytoskeleton remodeling. In embryos injected with $PI(3,4,5)P_3$/AM, the cleavage furrows assembled normally (Fig. 1 E). However, over the course of cellularization we observed a progressive disassembly of the myosin-II network, resulting in the multi-layering of nuclei and eventually in the formation of multinucleated cells (Fig. 1, E′, E″, and H; and Video 3). $PI(3,4,5)P_3$/AM-injected embryos showed no delay in

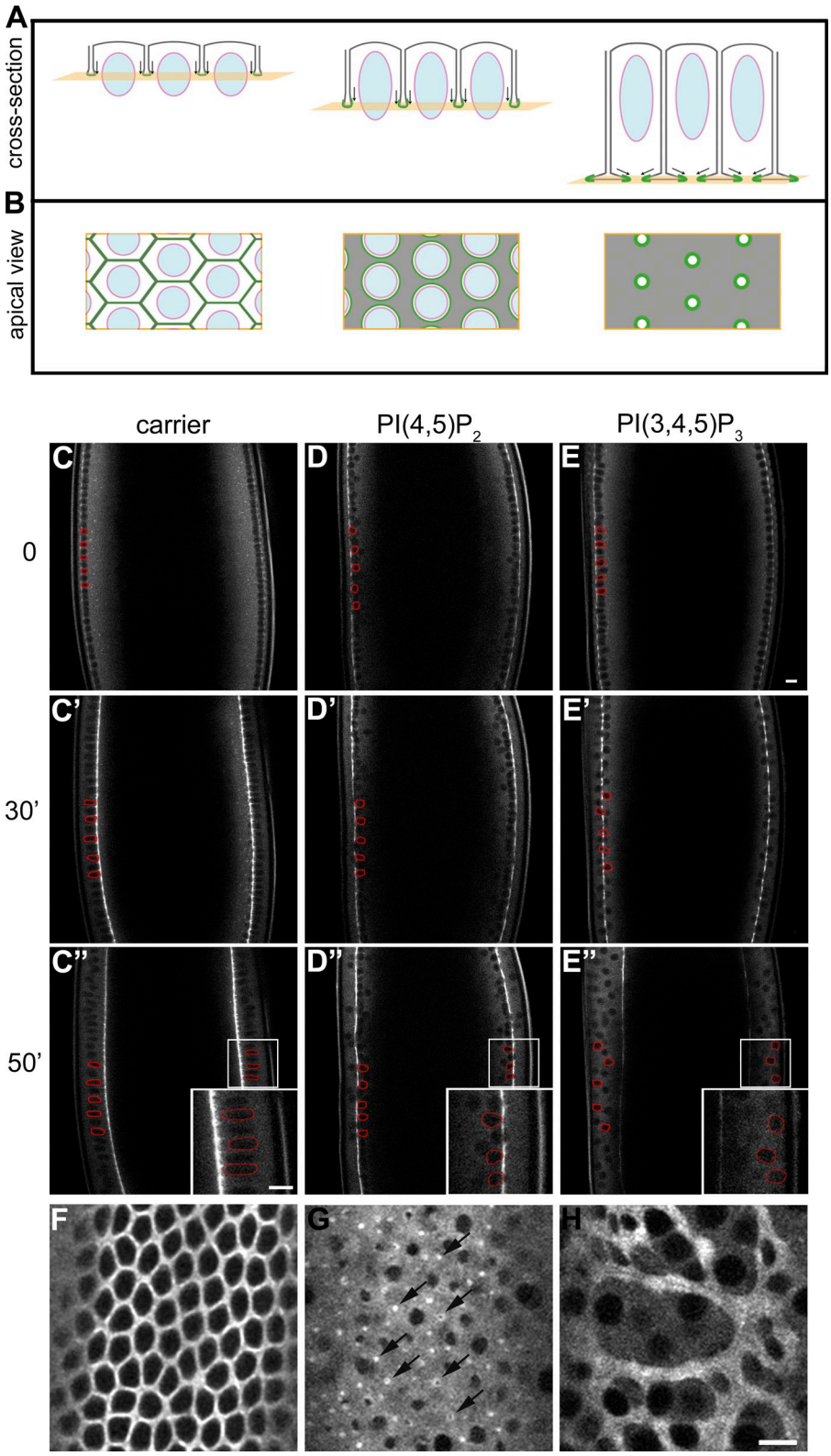

Figure 1. **Injection of plasma membrane phosphoinositides causes premature constriction ($PI(4,5)P_2$/AM) and disassembly ($PI(3,4,5)P_3$/AM) of the actomyosin network.** (A and B) Schematic summarizing the progression of cellularization in an optical cross section (A) and from a surface view at the plane of the actomyosin network (B). Note the changes in myosin organization (green) from the slow phase (left) to the fast phase/end of cellularization (right). See Introduction for details. (C–E″) Still frames from time-lapse two-photon movies of a cellularizing embryo expressing Sqh::GFP injected before the beginning of cellularization with: carrier (C, C′, and C″), $PI(4,5)P_2$/AM to a final concentration of 50 µM (D, D′, and D″), and $PI(3,4,5)P_3$/AM to a final concentration of 20 µM (E, E′, and E″). Three different time points are shown: 0 min (C, D, and E), 30 min (C′, D′, and E′), and 50 min (C″, D″, and E″). In control-injected embryos cleavage furrows are assembled and ingress normally (C, C′, and C″). In $PI(4,5)P_2$/AM-injected embryos nuclei remain trapped in hyper-constricted actomyosin rings and are pushed away from the epithelium into the interior of the embryo (D, D′, and D″). In $PI(3,4,5)P_3$/AM-injected embryos furrows are progressively disassembled, resulting in the formation of multinucleated cells and multi-layering (E, E′, and E″). In C–E″ some nuclei have been labeled in red to show their position with respect to the Sqh::GFP invaginating furrows. Insets in C″–E″ represent the magnified area of corresponding boxes. Bars, 10 µm. (F–H) Apical view of a cellularizing embryo expressing Sqh::GFP injected with: carrier (F), $PI(4,5)P_2$/AM (G), or $PI(3,4,5)P_3$/AM (H) taken 30 min (F and G) and 50 min (H) after the beginning of cellularization. Arrows show actomyosin hyper-constricted rings upon $PI(4,5)P_2$/AM injection. Bar, 10 µm.

the rate of plasma membrane invagination (Fig. 2, A″ and B″). Thus, the ectopic increase of $PI(4,5)P_2$ and $PI(3,4,5)P_3$ resulted in two different and complementary phenotypes: $PI(4,5)P_2$ promoted actomyosin contractility and shortening of the cells and $PI(3,4,5)P_3$ caused the disassembly of the actomyosin network and formation of multinucleated cells.

Increasing $PI(4,5)P_2$ levels during cellularization increases the stability and recruitment of myosin-II to the actomyosin network

A large body of experimental evidence has demonstrated that levels of myosin determine the contractile properties of

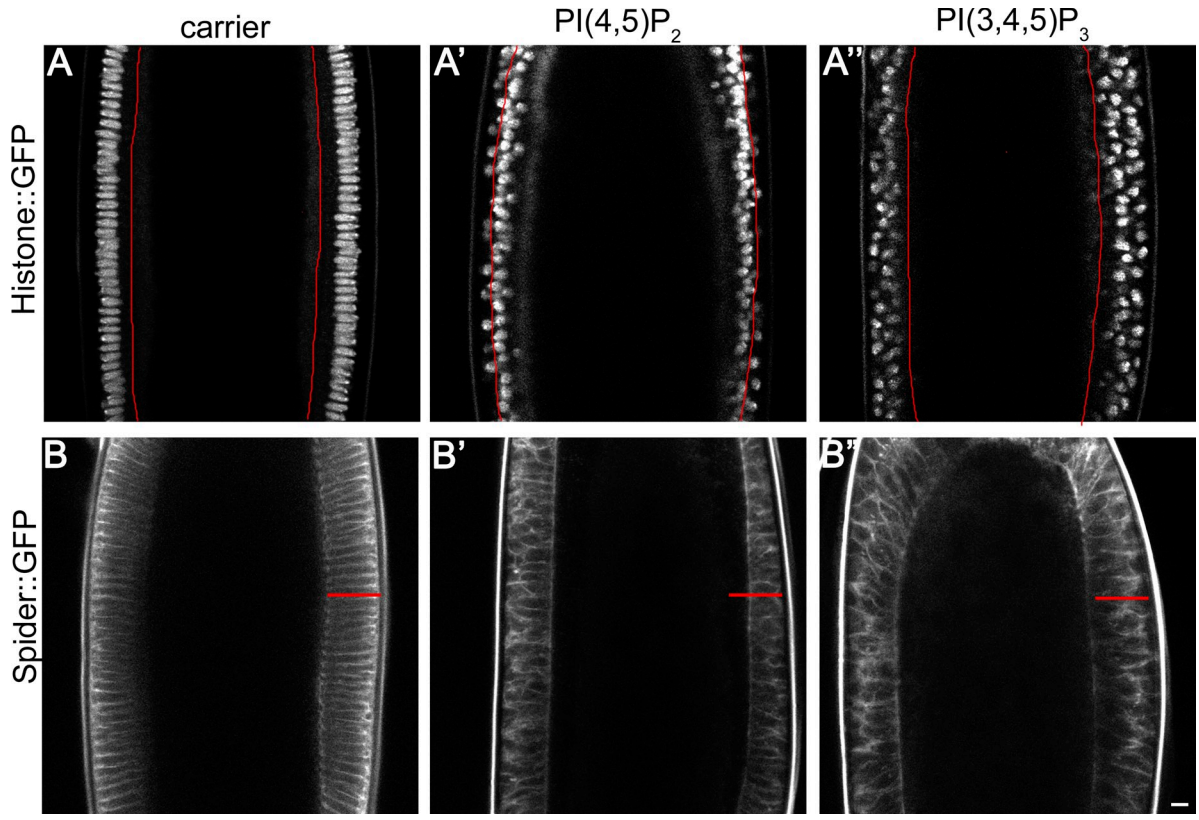

Figure 2. **PI(4,5)P_2/AM injection causes shortening of the cells and exclusion of nuclei from the epithelium.** (A–A″) Still frame from time-lapse two-photon movies of a cellularizing embryo expressing histone::GFP injected before the beginning of cellularization with: carrier (A), PI(4,5)P_2/AM (A′), and PI(3,4,5)P_3/AM (A″) taken 50 min after the beginning of cellularization. In control-injected embryos nuclei area attached at the cortex and elongate over the course of cellularization (A). In PI(4,5)P_2/AM-injected embryos, nuclei remain trapped in actomyosin hyper-constricted rings and are dragged toward the interior of the embryo (A′). PI(3,4,5)P_3/AM-injected nuclei do not elongate and detach from the cortex, resulting in multi-layering (A″). Red line indicates the furrow position in each condition. (B–B″) Still frame from time-lapse two-photon movies of a cellularizing embryo expressing Spider::GFP injected before the beginning of cellularization with: carrier (B), PI(4,5)P_2/AM (B′), and PI(3,4,5)P_3/AM (B″) taken 50 min after the beginning of cellularization. In control-injected embryos plasma membrane invaginates uniformly, giving rise to cells of ∼40 µm (B). In PI(4,5)P_2/AM-injected embryos, plasma membrane invaginates in an irregular manner, resulting in the formation of shortened cells (B′). PI(3,4,5)P_3/AM-injected embryos show no delay in the rate of plasma membrane invagination, although cells have an abnormal shape (B″). The red line in B′ and B″ indicates the cell length of the control-injected embryo shown in B. Bar, 10 µm.

actomyosin networks (Levayer and Lecuit, 2012). The concentration of myosin increases progressively from the beginning to the end of cellularization (Video 4), and myosin activity is absolutely required for the constriction of the actomyosin rings and basal closure (Royou et al., 2004). In agreement with a possible involvement of PI(4,5)P_2 in regulating the contractility of the actomyosin network, the PI(4,5)P_2 sensor PLCδ1-PH::GFP and Sqh::mCherry overlapped at the leading edge of the furrows over the entire course of cellularization (Fig. 3 A). To further test this hypothesis, we monitored the rate and turnover of Sqh::GFP in PI(4,5)P_2/AM-injected embryos. FRAP experiments performed in wild-type embryos showed that the recovery of Sqh::GFP fluorescence was significantly faster in embryos in the slow phase (early) than in the fast phase (late) of cellularization (Fig. 3 B and Videos 5 and 6). In early embryos, the recovery of Sqh::GFP fluorescence reached a plateau at 80% ± 2 of the pre-bleached level in 130 s, compared with 60% ± 1 recovery over the same time in late embryos. Thus, myosin-II is more stably associated with the actomyosin network during late cellularization than early cellularization. Analysis of FRAP experiments performed in early embryos injected with PI(4,5)P_2/AM revealed that the kinetics of recovery were significantly different from wild-type early embryos and very similar to wild-type embryos during fast phase (Fig. 3 B and Video 7) Thus, PI(4,5)P_2/AM injection causes the stabilization of myosin-II. Furthermore, starting from the onset of cellularization, Sqh::GFP levels were significantly higher in PI(4,5)P_2/AM-injected embryos than in control embryos (Fig. 3 C). Thus, increasing the levels of PI(4,5)P_2 causes an increase in the levels and stability of myosin-II, consistent with the hypothesis that PI(4,5)P_2 causes premature contraction of the actomyosin network.

PI(4,5)P_2 is required for assembly of the actomyosin network during early cellularization and for contractility during late cellularization

Having established that an increase in PI(4,5)P_2 levels causes the premature contraction of the actomyosin network, we next tested whether PI(4,5)P_2 was also required for actomyosin contractility. To control the endogenous plasma membrane levels of PI(4,5)P_2, we took advantage of the rapamycin-inducible dimerization system, which has been extensively used in cell culture

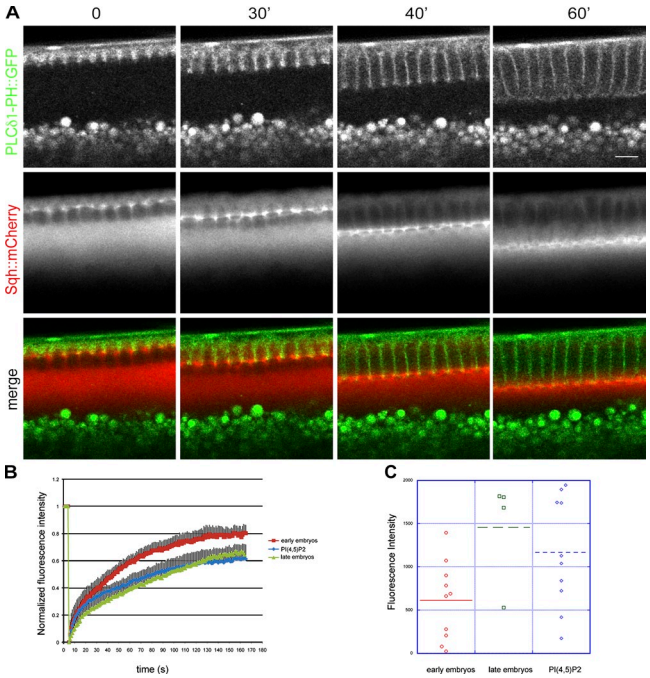

Figure 3. **PI(4,5)P_2/AM injection increases the stability and recruitment of myosin-II to the actomyosin network.** (A) Still frames from a time-lapse two-photon movie of a cellularizing embryo expressing the PI(4,5)P_2 sensor PLCδ1-PH::GFP (green) and Sqh::mCherry (red) showing the overlap between PI(4,5)P_2 and myosin-II over the course of cellularization (0, 30, 40, and 60 min). Note: the bright fluorescent spots below the cellularization front correspond to autofluorescence of yolk granules. Bar, 10 µm. (B) FRAP analysis in Sqh::GFP-expressing embryos. During the slow phase of cellularization the recovery rate of Sqh::GFP is much faster than during the fast phase, indicating that myosin-II is more stably associated at the furrow during late stages. In PI(4,5)P_2/AM-injected embryos the recovery rates during the slow phase are significantly slower than control-injected embryos and are comparable with the recovery rates of late embryos (Student's *t* test, P value = 7.76×10^{-15} for wild-type early embryos compared with PI(4,5)P_2-injected embryos; $n = 3$ embryos each condition). Errors bars represent mean ± SD. (C) Quantification of Sqh::GFP fluorescence intensity at the furrow in early embryos, late embryos, and PI(4,5)P_2-injected embryos. Sqh::GFP levels increase from early to late stages of cellularization. Injection of PI(4,5)P_2/AM causes a twofold increase in Sqh::GFP levels in early embryos (Student's *t* test, P = 0.039). Each dot represents an embryo. At least three independent experiments were quantified.

to translocate the inositol polyphosphate 5-phosphatase (5Ptase) to the plasma membrane in a temporally regulated manner and to convert PI(4,5)P_2 into PI(4)P (Suh et al., 2006; Varnai et al., 2006; Putyrski and Schultz, 2012). The rapamycin system is based on the heterodimerization of FRB (fragment of mammalian target of rapamycin) and FKBP12 protein domains (FK506 binding protein 12) in the presence of rapamycin (Muthuswamy et al., 1999). We first confirmed that this system could efficiently deplete PI(4,5)P_2 in *Drosophila* S2 cells by following the loss of plasma membrane localization of the PI(4,5)P_2 sensor, PLCδ1-PH-GFP (Fig. S2). We next generated transgenic flies coexpressing (a) the FRB domain coupled to the palmitoylation sequence of human GAP43, which serves as a plasma membrane anchor, (b) a truncated cytosolic form of the 5Ptase fused to the FKBP12 domain (Varnai et al., 2006), and (c) Sqh::GFP. In the absence of rapamycin, the 5Ptase remained cytosolic and cellularization proceeded normally (Fig. 4, A–D). Injection of rapamycin caused a rapid and efficient translocation of the 5Ptase to the plasma membrane (Fig. 4, E and I). When rapamycin was injected before the beginning of cellularization, the recruitment of the 5Ptase to the plasma membrane caused a progressive disassembly of the myosin network and arrest of plasma membrane invagination (Fig. 4, F–H). Injection of rapamycin after the onset of cellularization did not block plasma membrane invagination (Fig. 4, J and K). However, when the plasma membrane reached the base of the nuclei, the actomyosin network did not convert into contractile rings (Fig. 4 L). In control embryos, the area of the actomyosin rings was significantly smaller than the area of similar stage rapamycin-injected embryos (Fig. 4 L). Injection of rapamycin in embryos carrying the FKBP12 domain alone did not cause any visible cellularization phenotype (Fig. 4, M–P). Thus, PI(4,5)P_2 is essential for stabilizing the actomyosin network during early cellularization and for contractility after cells have reached their final length, during late cellularization.

PI(3,4,5)P_3 and Bottleneck antagonize PI(4,5)P_2 contractility during the slow phase of cellularization

The results presented above suggest that PI(4,5)P_2-mediated contractility is normally inhibited during the slow phase of cellularization. In fully polarized epithelial cells and in dividing cells, PI(4,5)P_2 and PI(3,4,5)P_3 are compartmentalized into distinct membrane domains where they exert different effects on actin organization (Insall and Weiner, 2001; Janetopoulos and Devreotes, 2006; Comer and Parent, 2007). Live imaging of embryos expressing the PI(3,4,5)P_3 sensor GFP::Akt-PH showed that PI(3,4,5)P_3 was detectable at the leading edge of the furrows only during the slow phase of cellularization (Fig. 5 A), indicating that PI(3,4,5)P_3 could be part of the mechanism counteracting actomyosin contractility. To test this hypothesis, embryos were injected with wortmannin, a PI-3 kinase inhibitor that blocks the conversion of PI(4,5)P_2 into PI(3,4,5)P_3. In wortmannin-injected embryos, the normal hexagonal pattern of tightly juxtaposed actomyosin arrays converted prematurely into actomyosin rings during the slow phase of cellularization (Fig. 5, C and E), recapitulating the PI(4,5)P_2-injected phenotype (Fig. 1 G). Loss of GFP::Akt-PH from the plasma membrane upon wortmannin injection confirmed inhibition of PI(3,4,5)P_3 production (Fig. S3, A–H). Importantly, injection of wortmannin before cycle 14 did not inhibit metaphase furrow formation and retraction (Fig. S3, I–L), thus demonstrating that PI-3 kinase activity is specifically required during the slow phase of cellularization, at the same time when the PI(4,5)P_2-induced phenotype is manifested.

The phenotype observed upon increasing the levels of PI(4,5)P_2 or decreasing the levels of PI(3,4,5)P_3 phenocopies the *bottleneck* mutation (Schejter and Wieschaus, 1993a; Fig. 5, F and G), suggesting that Bnk and PI(3,4,5)P_3 antagonize the contractile-promoting activity of PI(4,5)P_2 during the slow phase of cellularization. Multiple lines of evidence support this hypothesis. First, FRAP experiments performed in *bottleneck* mutant embryos demonstrated a slower recovery rate of Sqh::GFP compared with wild-type embryos (Fig. 6 A and Video 8) and similar to PI(4,5)P_2/AM-injected embryos (Fig. 3 B). In addition, the lack of Bnk caused the levels of Sqh::GFP during the

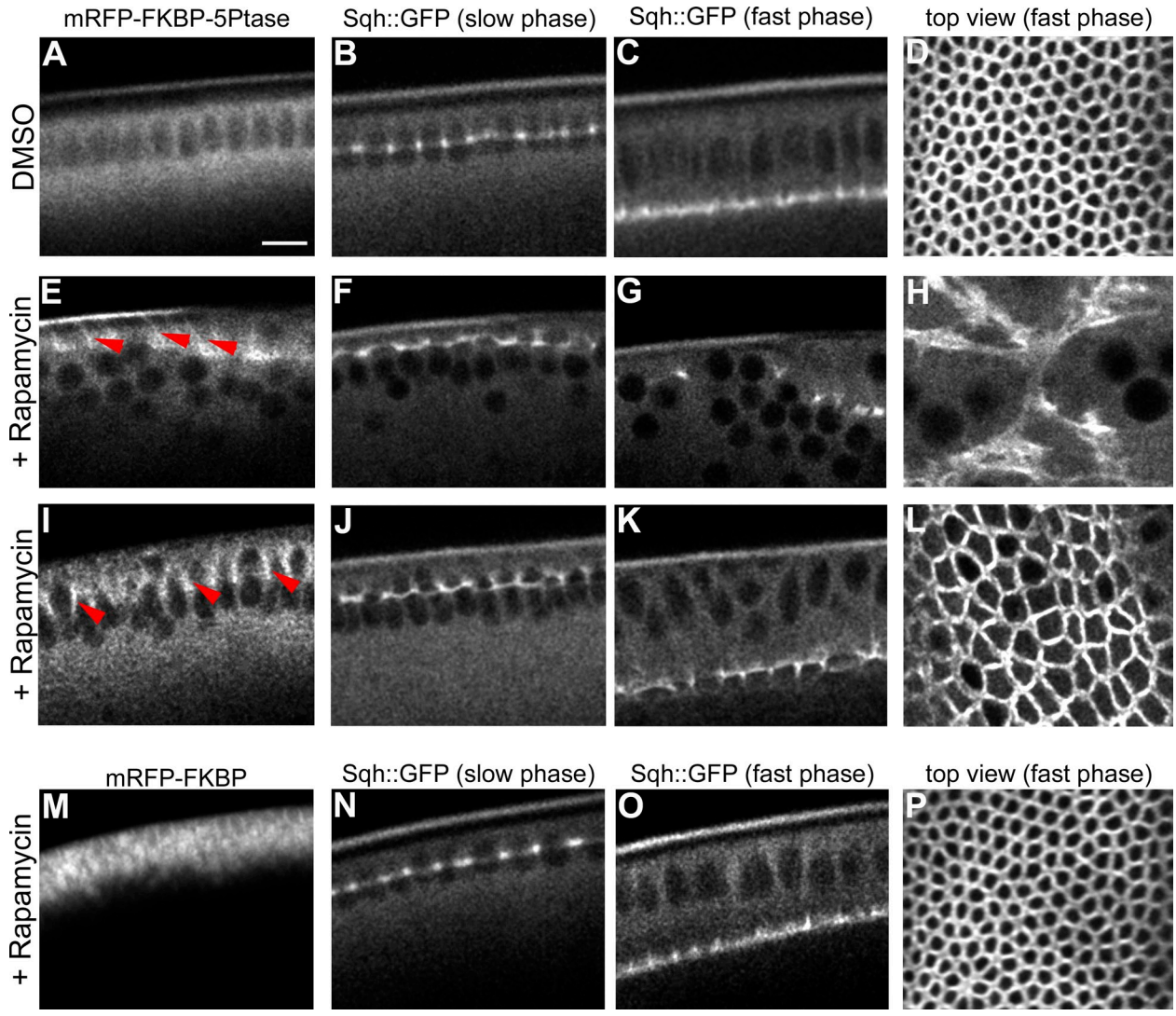

Figure 4. **Depletion of PI(4,5)P_2 from the plasma membrane leads to disassembly of the actomyosin network and arrests plasma membrane invagination.** (A–L) Still frames from time-lapse two-photon movies of embryos coexpressing the plasma membrane anchor FRB-CFP (CFP channel is not shown), mRFP-FKBP-5Ptase, and Sqh::GFP. Rapamycin was injected during cycle 13 (E–H) and at the onset of cellularization (I–L). (A–D) In control (DMSO)-injected embryos the 5Ptase remains cytosolic (A) and furrows ingress without any visible alternation (B–D). (E–H) Injection of rapamycin during cycle 13. Upon recruitment of the 5Ptase to the plasma membrane (E, red arrowheads), Sqh::GFP is progressively disassembled over the course of cellularization (F and G). Apical view illustrating the disorganization of the actomyosin network during fast phase (H). (I–L) Rapamycin injection at the onset of cellularization. The 5Ptase is recruited to the plasma membrane (I, red arrowheads), and furrows are assembled (J) and ingress normally (K). Apical view: during the fast phase the area of the actomyosin rings in rapamycin-injected embryos (L) is double the area of similar stage control-injected embryos (D; control = 11.96 ± 1.34 μm^2, $n = 5$; rapamycin = 22.76 ± 7.11 μm^2, $n = 3$; Student's t test, $P = 2.74 \times 10^{-8}$). (M–P) Injection of rapamycin in control embryos expressing the plasma membrane anchor FRB-CFP (CFP channel is not shown) and the FKBP construct lacking the 5Ptase catalytic domain (M) demonstrates that the morphology and dynamics of the actomyosin network is not altered upon rapamycin injection (N–P). Bar, 10 µm. See also Fig. S2.

slow phase to increase up to the levels present during fast phase in wild-type embryos (Fig. 6 B), again like in PI(4,5)P_2/AM-injected embryos. Second, Bnk colocalized with both the PI(4,5)P_2 and PI(3,4,5)P_3 sensors to the actomyosin network of early cellularizing embryos (Fig. 6, C–N). Third, PIP strip binding and lipid flotation assays revealed that Bnk interacted with PI(3,4,5)P_3 and to a lesser extent with PI(4,5)P_2 (Fig. 7, A–D). Fourth, FRAP measurements in embryos expressing YFP::Bnk under its endogenous promoter demonstrated that in wortmannin-injected embryos the recovery rate of Bnk fluorescence was significantly faster (approximately two times) than in control-injected embryos (Fig. 7 E and Videos 9 and 10), thus showing that PI(3,4,5)P_3 production controls Bnk turnover at the furrow. Furthermore, injection of PI(3,4,5)P_3/AM at the onset of cellularization resulted in increased Bnk recruitment (Fig. S4, A–E). Consistent with the rapid degradation of Bnk during the fast phase (Schejter and Wieschaus, 1993a), loss of Bottleneck did not appear to be affected upon PI(3,4,5)P_3/AM injection (Fig. S4, C–F). Taken together, these data suggest that Bottleneck acts downstream of PI(3,4,5)P_3 in counteracting PI(4,5)P_2-mediated actomyosin contractility during the slow phase.

Bottleneck acts as a cross-linker/stabilizer of actin filaments

The *bottleneck* mutant phenotype suggests a putative role for Bnk in regulating the sliding of actomyosin filaments to prevent

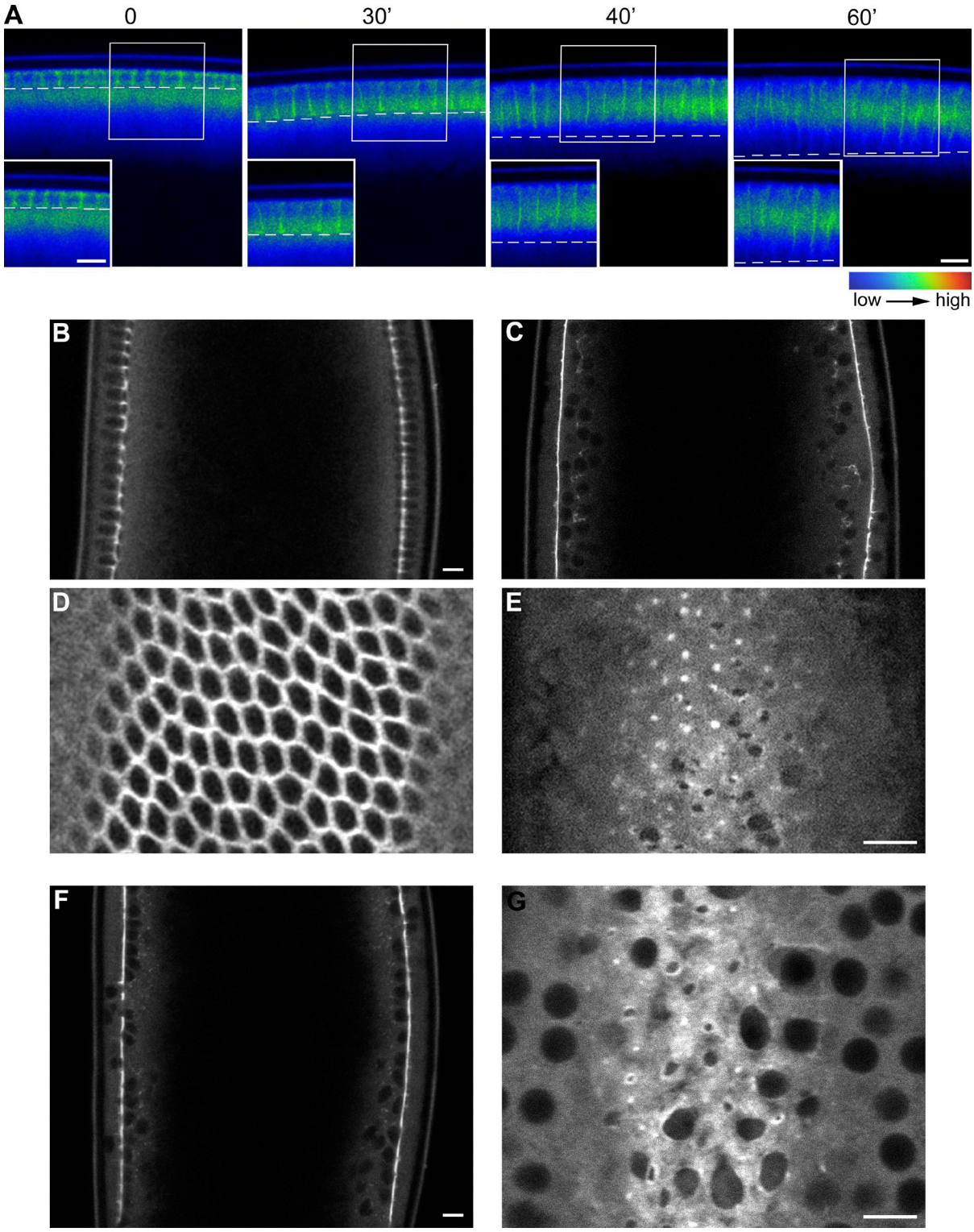

Figure 5. **Injection of wortmannin causes premature constriction of the actomyosin rings.** (A) Still frames from a time-lapse two-photon movie of a cellularizing embryo showing the localization of the PI(3,4,5)P_3 sensor GFP::AKT-PH. The dashed line indicates the position of the furrow; GFP::AKT-PH is present at the furrows at early time points (0 and 30 min) and disappears at later stages (40 and 60 min). Insets show higher magnification of boxed areas. Grayscale 8-bit still images were pseudo-colored with the rainbow LookUp Table (LUT; ImageJ software) to produce false-color images. Pixels with a value of 0 are black and pixels with a value of 255 are red. Bars, 10 µm. (B–E) Still frame from a two-photon movie of a control (DMSO)-injected embryo taken after 20 min from the onset of cellularization (B) and of an embryo injected with wortmannin (C). (D and E) Apical view of the same control- and wortmannin-injected embryos. Wortmannin injection causes the premature conversion of the hexagonal actomyosin arrays into contractile rings recapitulating the PI(4,5)P_2-injected and *bottleneck* mutant phenotypes. Bars, 10 µm. (F) Still frame from a two-photon movie of an embryo expressing Sqh::GFP injected with siRNA against Bnk during cycle 10, when the protein starts to be expressed. Bottleneck depletion causes premature contraction of the actomyosin network during early cellularization, resulting in a phenotype that is very similar to the PI(4,5)P_2/AM/wortmannin-induced phenotype. Bar, 10 µm. (G) Apical view of the same embryo. Bar, 10 µm.

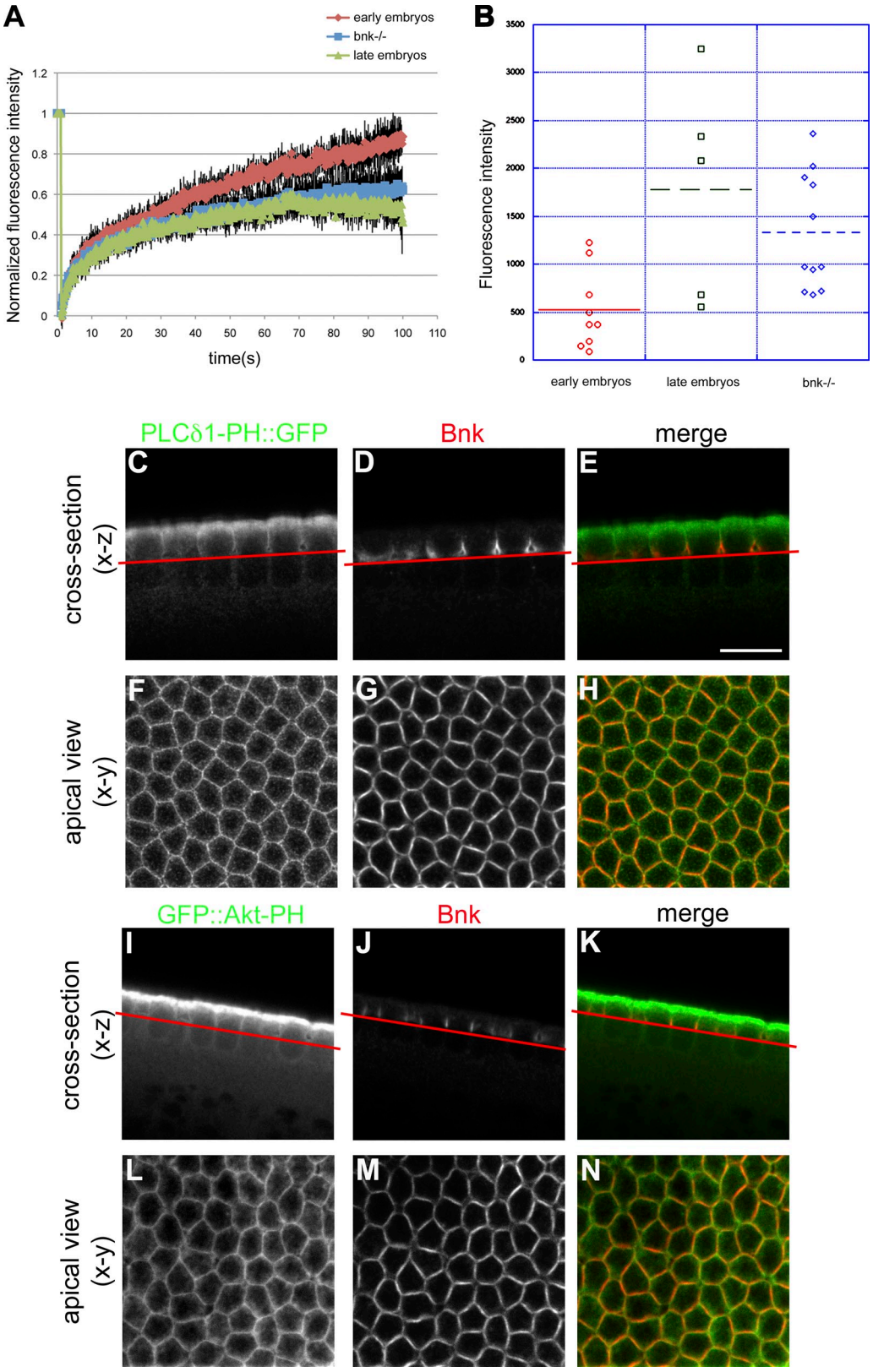

Figure 6. ***bottleneck* mutant embryos display increased stability and recruitment of myosin-II to the furrows.** (A) FRAP experiments in *bottleneck* mutant embryos (Df(3R)tll^{e}) expressing Sqh::GFP. In *bottleneck* mutant embryos the recovery rates of Sqh::GFP are slower than wild-type early embryos and similar to wild-type embryos during late stages. Quantification of three independent FRAP experiments is plotted (Student's *t* test, $P = 2.98 \times 10^{-34}$ wild-type early compared with Df(3R)tll^{e} embryos). Errors bars represent mean ± SD. (B) Quantification of Sqh::GFP fluorescence intensity at the furrow in early embryos, late embryos, and *bottleneck* mutant embryos. In *bottleneck* mutant embryos the levels of Sqh::GFP are significantly up-regulated (approximately threefold) compared with similar stage wild-type early embryos (Student's *t* test, P = 0.0048) again like in $PI(4,5)P_2$/AM-injected embryos. Each dot represents an embryo. At least three independent embryos were quantified. (C–H) Representative confocal sections of an embryo expressing the $PI(4,5)P_2$ sensor PLCδ1-PH::GFP,

ring contraction. One way to test this hypothesis would be to assess Bnk activity in actin polymerization/contractility in vitro assays using recombinant, purified proteins. However, as bacterially expressed recombinant Bnk is insoluble, we used a heterologous cell culture system that would mimic the transient expression of Bnk during cellularization. HeLa cells, which do not endogenously express Bnk, were transfected with Bnk tagged with mCherry. The result of this experiment demonstrates that mCherry::Bnk localized primarily to long cytoplasmic filaments aligned along the longitudinal axis of the cells (Fig. 8 A). These filaments resembled stress fibers, contractile actomyosin filaments involved in cell migration. To confirm the nature of the Bnk-decorated filaments, HeLa cells expressing Bnk were co-stained with fluorescently labeled phalloidin, a compound that binds specifically to filamentous actin. Fig. 8, A and B show that Bnk and phalloidin completely colocalized. This staining also revealed that the levels of actin on stress fibers were drastically up-regulated in Bnk-expressing cells (to the extent that imaging phalloidin with the same setting as in control cells resulted in a complete saturation of the signal; Fig. 8 C). To exclude the possibility that Bnk expression induces a conformational change in actin filaments that allows more phalloidin binding, HeLa cells were cotransfected with the actin-binding peptide Lifeact (Riedl et al., 2008) and Bnk. As shown in Fig. S5, A and B, expression of Bnk caused the formation of Lifeact-positive filaments that were thicker compared with Lifeact-only transfected cells. Unlike actin, myosin-II levels were not up-regulated upon Bottleneck expression (Fig. 8 D). Treatment of HeLa cells with cytochalasin D and latrunculin A, two actin-depolymerizing drugs, showed that in Bnk-expressing cells stress fibers were resistant to both treatments, whereas in nontransfected cells stress fibers disassembled completely within 15 min (Fig. 8 E and Fig. S5, E–L). Thus, Bnk expression causes the stabilization of stress fibers leading to the assembly of thick filaments with a high actin/myosin ratio.

Collectively, these data show that PI(4,5)P_2 contractility is counteracted by Bnk and PI(3,4,5)P_3, which act by limiting myosin-II recruitment and by stabilizing actin filaments in an interconnected array. Increasing the levels of PI(4,5)P_2 causes more myosin-II recruitment and premature contraction. Likewise, decreasing the levels of PI(3,4,5)P_3 or Bnk prematurely unlocks PI(4,5)P_2 contractility, causing the formation of shortened cells with abnormal shape (Fig. 9, see model).

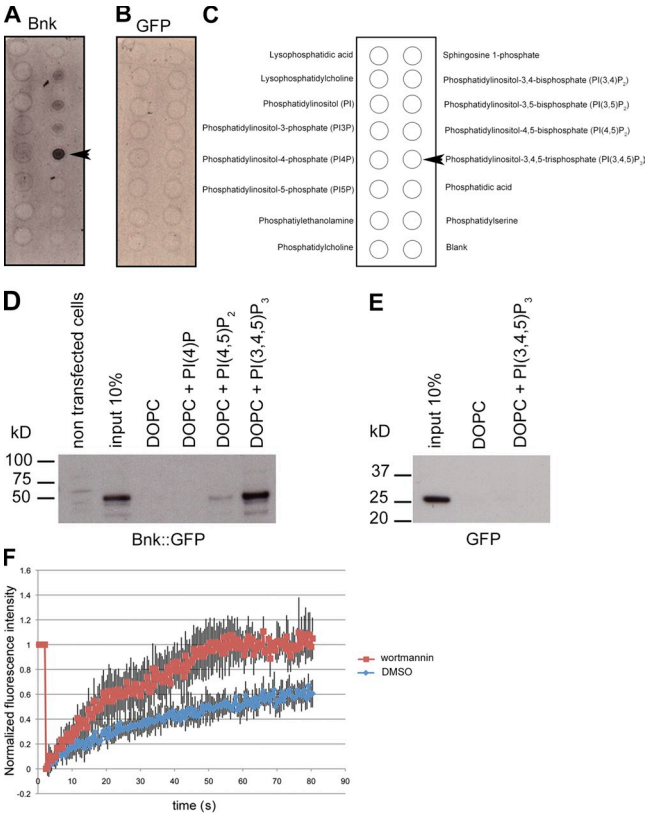

Figure 7. **Bottleneck binds to PI(3,4,5)P_3 and PI3-kinase activity is required to stabilize Bottleneck at the furrows.** (A–C) PIP strips binding assays. ^{35}S-radiolabeled Bnk or ^{35}S-radiolabeled GFP (as a control) were incubated with PIP strips. After extensive washes, membranes were dried and exposed on an x-ray film at room temperature. Bottleneck interacts with PI(3,4,5)P_3 and to a less extent with PI(4,5)P_2, PI(3,4)P_2, and PI(3,5)P_2. A schematic representation of the lipids spotted on the membrane is shown (C). Arrowheads in A and C point to the PI(3,4,5)P_3 position. (D and E) Liposome flotation assay. HeLa cells expressing Bnk::GFP were lysed and incubated with either liposomes alone (DOPC) or with liposomes containing PI(4)P or PI(4,5)P_2 or PI(3,4,5)P_3. Liposomes were floated by centrifugation in a sucrose gradient and the top layer was loaded on an SDS-PAGE. Western blot using an anti-GFP antibody shows binding of Bnk to PI(3,4,5)P_3 and to a lesser extent to PI(4,5)P_2 (n = 3). Lysate of HeLa cells expressing GFP was used as negative control (E). (E) FRAP analysis in embryos expressing Bnk::YFP under its endogenous promoter shows that in wortmannin-injected embryos, the Bnk fluorescence recovery rate is significantly faster than in control-injected embryos. For example, although in wortmannin-injected embryos the fluorescence was completely recovered after 60 s, in control-injected embryos, at this time point only 50% of the initial fluorescence was recovered. (Student's t test, $P = 3.28 \times 10^{-35}$; $n = 5$ embryos for each condition). Errors bars represent mean ± SD.

Discussion

A fundamental question underlying cell and tissue morphogenesis is how different types of actomyosin networks polymerize on specific plasma membrane domains and contract in a spatio-temporally coordinated manner in order to produce cell shape changes. The results presented here elucidate a regulatory mechanism linking actomyosin contractility with plasma membrane expansion during the morphogenesis of an epithelial tissue, the formation of the *Drosophila* cellular blastoderm. This mechanism is based on the temporal modulation of PI(4,5)P_2-dependent

which was fixed and stained with anti-GFP (C) and anti-Bnk (D) antibodies. Cross sections (C–E) and apical view (F–H) are shown, illustrating the colocalization (yellow) between PLCδ1-PH::GFP (green) and Bottleneck (red) during the slow phase of cellularization (E–H). (C–E) Red line indicates the focal plane at which the apical view was imaged. (I–N) Representative confocal sections of an embryo expressing the PI(3,4,5)P_3 sensor GFP::AKT-PH, which was fixed and stained with anti-GFP (I) and anti-Bnk (J) antibodies. Cross sections (I–K) and apical view (L–N) are shown, illustrating the colocalization (yellow) between GFP::AKT-PH (green) and Bottleneck (red) during the slow phase of cellularization (K and N). Red line in I–K indicates the focal plane at which the apical view was imaged. Bars: (all panels) 10 µm.

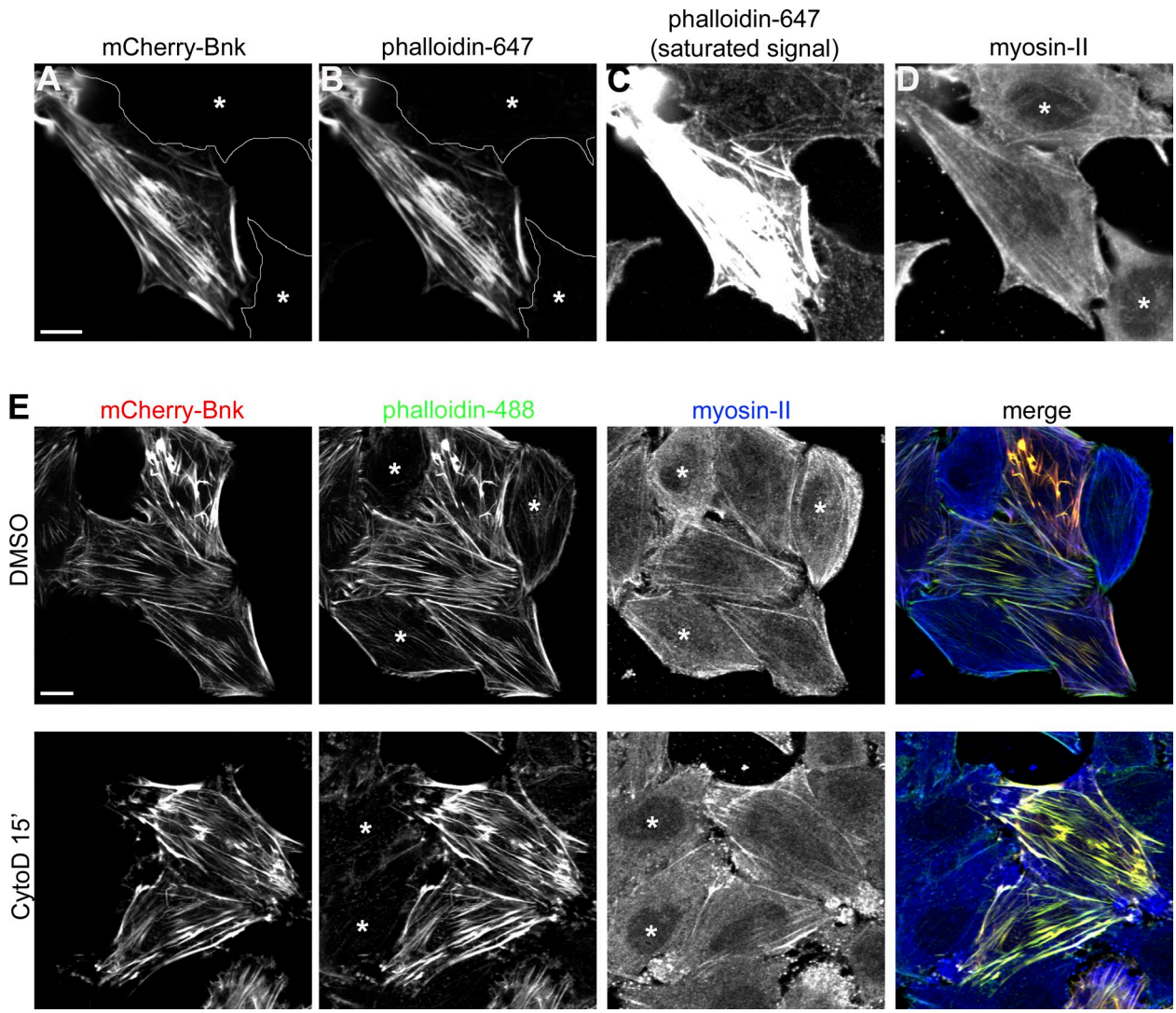

Figure 8. **Bottleneck acts as a cross-linker/stabilizer of actin filaments.** (A–D) Confocal images of HeLa cells expressing mCherry-Bnk (A) stained with phalloidin 647 (B and C) and myosin-II antibody (D) showing the colocalization between Bnk and actin. Nontransfected cells are marked with an asterisk. C shows the assembly of actin filaments in Bnk-overexpressing cells. In this panel, the phalloidin signal was adjusted to visualize actin in nontransfected cells. This resulted in the saturation of the phalloidin signal in the Bnk-transfected cell. Bar, 10 µm. (E) Confocal images of HeLa cells treated with cytochalasin D for 15 min, fixed, and stained with phalloidin 488 and myosin-II antibody. In Bnk-transfected cells, stress fibers do not depolymerize. DMSO-treated cells are shown as a control. Asterisks indicate nontransfected cells. Bar, 10 µm. See also Fig. S5.

actomyosin contractility by $PI(3,4,5)P_3$ and Bottleneck. Our data argue that $PI(4,5)P_2$ is required for assembling the actomyosin network at the plasma membrane during the initial stages of cellularization. During the slow phase of plasma membrane invagination, $PI(4,5)P_2$-dependent contractility is counteracted by the presence of $PI(3,4,5)P_3$. During the fast phase, $PI(3,4,5)P_3$ levels decrease, allowing $PI(4,5)P_2$ to carry out its function on actomyosin contraction.

The morphological abnormalities resulting from increasing $PI(4,5)P_2$ or decreasing $PI(3,4,5)P_3$ levels point toward a different requirement for these two phosphoinositides on actomyosin organization. Although blocking $PI(4,5)P_2$ conversion into $PI(3,4,5)P_3$ with wortmannin should lead, in principle, to an increase in $PI(4,5)P_2$ levels, this increase should be minimal compared with the endogenous abundance of $PI(4,5)P_2$ in biological membranes. Indeed, estimates from a variety of different systems indicate that $PI(3,4,5)P_3$ is only ~2–5% of $PI(4,5)P_2$ (Balla, 2013). Therefore, it appears more likely that the premature contraction observed in wortmannin-treated embryos is due to a lack of $PI(3,4,5)P_3$ rather than an increase in $PI(4,5)P_2$ levels. $PI(3,4,5)P_3$ might control actin polymerization in such a way that the actomyosin network acquires the conformation of an hexagonal array of dense actin bundles. During the slow phase, $PI(3,4,5)P_3$ is required to stabilize Bnk at the furrow, which, in turn, prevents the sliding of actomyosin filaments, presumably by acting as an actin cross-linker. Cross-linked actin filaments might be less accessible to myosin-II or, alternatively, steric hindrance by Bnk itself might prevent the incorporation of myosin-II. Consistent with this hypothesis, the expression of Bnk in HeLa cells causes the stabilization of stress fibers leading to the assembly of thick filaments with a high actin/myosin ratio. Furthermore, both *bottleneck* mutant and $PI(4,5)P_2$-injected embryos are associated with increased recruitment and stabilization of myosin-II during early cellularization, reaching the levels present

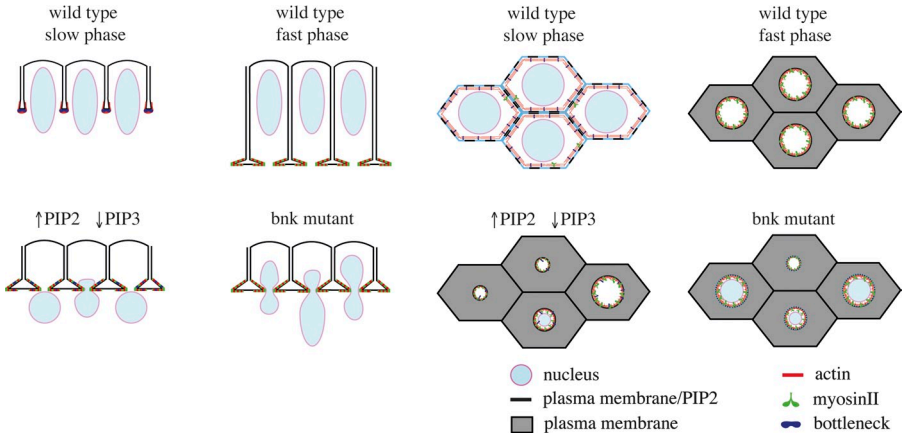

Figure 9. **Model illustrating temporal modulating of PI(4,5)P_2-dependent actomyosin contractility during tissue morphogenesis.** In each horizontal row, the left two cartoons correspond to optical cross section and the right two cartoons correspond to apical view at the level of the actomyosin network. (Top row) During the slow phase, PI(4,5)P_2 (black) is required for the assembly and adhesion of the network to the plasma membrane. PI(4,5)P_2 contractility is opposed by the presence of PI(3,4,5)P_3 (light blue) and Bottleneck (dark blue). PI(3,4,5)P_3 is required for keeping the network interconnected and organized in a matrix of dense actin bundles (red) with a relative low concentration of myosin-II. Bottleneck contributes to stabilizing the network by cross-linking actin filaments and by limiting the incorporation of myosin-II (green). During the fast phase, the decrease in PI(3,4,5)P_3 levels and degradation of Bottleneck (Schejter and Wieschaus, 1993a) allow PI(4,5)P_2-dependent contractility and basal closure. (Bottom row) An increase in PI(4,5)P_2 or a decrease in PI(3,4,5)P_3 levels during the slow phase causes premature contraction and formation of shortened cells with nuclei trapped in actomyosin rings recapitulating the *bottleneck* mutant phenotype.

during late cellularization, when the actomyosin network is converted into contractile rings. Similarly, the contraction of cytokinetic rings in cell culture is also associated with an increased stability of myosin-II in the equatorial cortex (Uehara et al., 2010). It is therefore likely that these changes in myosin-II are the ultimate cause of premature contraction. In addition, hydrolysis of PI(4,5)P_2 into DAG and IP_3 might also contribute to contractility by increasing intracellular calcium and activation of myosin light chain kinase (Wong et al., 2005).

In contrast to the PI(4,5)P_2-induced phenotype, the cellularization phenotype induced upon increasing the levels of PI(3,4,5)P_3 is characterized by a disassembly of the actomyosin network and formation of multinucleated cells, recapitulating the *nullo* and *serendipity-α* zygotic mutant phenotype (Schweisguth et al., 1990; Simpson and Wieschaus, 1990). Taken together, our results are therefore consistent with a model in which PI(4,5)P_2 and PI(3,4,5)P_3 play distinct roles during morphogenesis. Recent data suggest that PI(4,5)P_2 and PI(3,4,5)P_3 are compartmentalized in different plasma membrane domains during cell polarization (Gassama-Diagne et al., 2006; Martin-Belmonte et al., 2007). PI(3,4,5)P_3 localizes at the leading edge of migrating cells where it promotes lamellipodia formation, whereas PI(4,5)P_2 accumulates at the rear (Arrieumerlou and Meyer, 2005; Janetopoulos and Devreotes, 2006). The distribution of PI(4,5)P_2 and PI(3,4,5)P_3 seems to be polarized also during cytokinesis, with PI(4,5)P_2 enriched at the cleavage furrow and PI(3,4,5)P_3 enriched at the poles, at least in some cell types (Field et al., 2005; Janetopoulos and Devreotes, 2006). In polarized epithelial cells, PI(4,5)P_2 is localized to the apical surface and PI(3,4,5)P_3 to the basolateral plasma membrane (Comer and Parent, 2007). Our results demonstrate that during cellularization, PI(4,5)P_2 is present at the apical surface but is also localized at the basolateral surface and at the leading edge of the furrows. Similarly, PI(3,4,5)P_3 is enriched at the basolateral surface but is also present at the apical surface. This might indicate that the newly forming cells are not yet fully polarized, or it might reflect the complex state of the plasma membrane during a process in which cytokinesis is coupled with the establishment of apical–basal polarity. Indeed, strict apical and basolateral domains might not be established until apical adherens junctions assemble toward the end of cellularization. However, whether a compartmentalized mode of action can be generalized to all morphogenetic processes in which PI(4,5)P_2 and PI(3,4,5)P_3 are involved awaits further experimentation. The development of new probes that would allow direct visualization and quantification of phosphoinositide concentrations in living cells and organisms will undoubtedly provide important insights into the function of this class of lipids during morphogenesis.

The balance between PI(4,5)P_2 and PI(3,4,5)P_3 is controlled by class-I phosphatidylinositol 3-kinase (PI3-kinase), which phosphorylates PI(4,5)P_2 to PI(3,4,5)P_3, and by the 3-phosphate PTEN (phosphatase and tensin homologue), which converts PI(3,4,5)P_3 back to PI(4,5)P_2 (Stambolic et al., 1998). It is therefore likely that the activity of these two enzymes is specifically regulated during cellularization in such a way that PI(3,4,5)P_3 levels at the leading edge of the furrows are higher during the slow phase. The decrease in PI(3,4,5)P_3 levels is concomitant with the disassembly of basal junctions and assembly of apical adherens junctions. Adherens junctions might modulate PI(4,5)P_2/PI(3,4,5)P_3 levels by controlling plasma membrane recruitment of PTEN (von Stein et al., 2005; Pinal et al., 2006) and/or PI3-kinase. Interestingly, PTEN mutant embryos display several defects in cortical actin organization and slower cellularization kinetics. The interpretation of this phenotype is, however, complicated by the additional requirement of PTEN in controlling nuclear migration and axial expansion during preblastoderm stages (von Stein et al., 2005). A more precise spatiotemporal modulation of PTEN activity will undoubtedly help clarify its specific role during cellularization.

In conclusion, the results presented in this study suggest a mechanism for temporally modulating the activity of PI(4,5)P_2 during tissue morphogenesis. This mechanism coordinating actomyosin contraction with plasma membrane expansion ensures that cells of the correct size and shape are generated (Fig. 9, see model). The downstream cell biological basis underlying this coordination remains to be elucidated. Because membrane tension regulates both endocytosis and exocytosis (Apodaca, 2002; Boulant et al., 2011; Gauthier et al., 2011) and because

endocytosis and exocytosis are both required to complete cellularization (Sisson et al., 2000; Pelissier et al., 2003; Sokac and Wieschaus, 2008; Fabrowski et al., 2013; Lee and Harris, 2013), increased actomyosin contractility might counteract plasma membrane expansion by altering endo-exocytic activities at the plasma membrane. Further experiments will be required to test whether this is the case.

Given the importance of actomyosin contraction in cell shape changes the results of our analysis could have important implications for understanding the temporal regulation of other types of actomyosin networks underlying the morphogenesis of multicellular systems.

Materials and methods

Fly stocks

Wild-type flies were Oregon-R; all stocks were maintained by standard methods at 25°C unless otherwise specified.

yw*, sqh^{AX3}; P[w+, sqh>sqh::GFP.RLC] (Royou et al., 2004; stock no. 42235, Bloomington Drosophila Stock Center). The *sqh* ORF C-terminally tagged with GFP was cloned into the P transformation vector pCasPer downstream of the *sqh* endogenous promoter (−1,328 bp from start codon).

w*;; P[w+, sqh>sqh::mCherry^{A11}] (Martin et al., 2009). A 2-kb genomic fragment containing the *squ* promoter and ORF C-terminally tagged with mCherry and fused to the *sqh* 3′ untranslated region (800 base pairs) was cloned into CasPer4.

w*;; P[w+, H2AvGFP] (a gift from E. Wieschaus, Princeton University, Princeton, NJ); a 4.1-kb BglII *His2AvD* genomic fragment in which GFP was C-terminally fused to the *His2AvD* coding sequence and cloned into a CaSper4-based vector.

y,w*;;P[w+, PTT-un1]gish^{spider} (Morin et al., 2001). GFP is inserted into the *spider* locus. The exact location is unknown.

w*;P[w+,btl>Gal4, UAS>PLC-PH::GFP] (a gift from Maria Leptin, EMBL, Heidelberg, Germany). The PLC-PH domain, corresponding to residues 11–170 of human PLCδ1, fused C-terminally to GFP was cloned into a CaSper-based transformation vector.

w*;;P[w+, UASp>GFP::AKT-PH] (this paper). The mouse AKT-PH domain residues 1–441, fused C-terminally to GFP, was cloned into pPW vector (Drosophila Genomics Resource Center, Bloomington, IN).

w*,P[w+, UASp>mRFP::FKBP-5Ptase. The human FKBP12-coding sequence fused N-terminally to mRFP and C-terminally to human type IV 5Ptase catalytic domain (residues 214–644 in which the C641A mutation was introduced to destroy the C-terminal CAAX domain) was cloned into pPW vector (Drosophila Genomics Resource Center).

w*;;P[w+, UASp>Lck-FRB::CFP]. The FRB domain corresponding to residues 2019–2114 of human mTOR1 was fused N-terminally to residues 1–20 of human GAP43 and C-terminally to CFP and cloned into pPW vector (Drosophila Genomics Resource Center).

w*;; P[w+, 2kbBnk5′>YFP::Bnk-3′UTR]. N-terminal YFP tagged Bottleneck (YFP::Bnk) was cloned under the control of its endogenous promoter (−2,017 bp from the start codon) and 3′UTR (+768 from stop codon) into the P transformation vector CasPerR5.

Df(3R)tll^{e},ca[1]/TM6B,Tb[1]ca[1] (Bloomington Drosophila Stock Center, stock no. 5415). This is the deficiency covering the *bottleneck* locus that has been used in this study.

w*; P[w+,matαTub>Gal4::VP16]; [w+, mat αTub>Gal4:: VP16]. The maternal tubulin promoter (1.5 kb upstream of the first ATG) was cloned in front of the GAL4VP16 coding sequence into a CaSper-based vector.

Cloning and antibody generation

All constructs were cloned into the pPW vector (Drosophila Genomics Resource Center) using the Gateway cloning system (Life Technologies) according to standard procedures. The antibody against Bnk was raised in rat (Eurogentec). Full-length Bottleneck cDNA was cloned into the His-tagged Gateway pDEST17 vector (Invitrogen) and protein was purified from inclusion bodies under denaturing conditions (6 M Urea) using Ni-NTA agarose beads (QIAGEN). N-terminal YFP-tagged Bottleneck (YFP::Bnk) was cloned under the control of its endogenous promoter (−2,017 bp from the start codon) and 3′UTR (+768 from stop codon) into the P transformation vector CasPerR5, which carries in the selectable marker *mini-white*$^{+}$. Transgenic flies were obtained by standard methods.

PI(4,5)P_2/AM and PI(3,4,5)P_3/AM synthesis

All chemicals were purchased from Sigma-Aldrich except enantiopure, which was purchased from SiChem. PI(4,5)P_2/AM and PI(3,4,5)P_3/AM were synthetized as described previously (Laketa et al., 2009). In brief, for the synthesis of membrane-permeant PI(4,5)P_2, enantiomerically pure 3,6-di-*O*-butyryl-1,2:4,5-di-*O*-cyclohexylidene-myo-inositol was treated with acid to remove the more labile trans-ketale. The resulting diol was phosphorylated with a phosphorous(III) reagent (dibenzyl-*N*,*N*-diisopropyl phosphoramidite) in the presence of tetrazole, followed by oxidation to bisphosphate at −78°C. Subsequently, the second ketale was removed and the axial hydroxy group was selectively esterified with butyric acid via an orthoester intermediate. The resulting alcohol was reacted with a 1,2-di-*O*-octanoyl-glycerol (benzyl)-*N*,*N*-diisopropyl phosphoramidite. Oxidation then provided a fully protected PIP_2 derivative, which was subjected to deprotection by hydrogenolysis on a palladium catalyst in glacial acetic acid. After freeze-drying the lipid was subjected to alkylation by acetoxymethyl bromide in acetonitrile and diisopropylethylamine to give the desired membrane-permeant PIP_2. For the synthesis of membrane-permeant PI(3,4,5)P_3, the butyrate in the 3-*O* position was selectively removed by treatment with diisopropylethylamine in methanol at 37°C. After removal of the labile trans-ketale, the resulting three free hydroxy groups were phosphorylated as described above. All further steps proceeded highly similar to the synthesis of the PI(4,5)P_2 derivative. The chemico-physical properties of the final molecules and all intermediates were fully characterized by NMR, mass spectrometry, and chromatography.

Embryo injections and two-photon microscopy

PI(4,5)P_2/AM and PI(3,4,5)P_3/AM were injected at the concentration of 2 mM and 1 mM, respectively, in a solution of 30% DMSO in PBS. The dilution factor upon injection in a *Drosophila* embryo is ∼1:50; therefore, the estimated final concentration in the embryos is ∼40 µM for PI(4,5)P_2 and ∼20 µM for PI(3,4,5)P_3. Wortmannin (Sigma-Aldrich) was injected at the concentration of 5 µM in DMSO (final concentration ∼100 nM). Rapamycin (LC Laboratories) was injected at the concentration of 5 mM in DMSO (final concentration ∼100 µM). All compounds were injected in the posterior pole of the embryos. Embryos were dechorionated with 50% sodium hypochlorite solution, aligned and positioned on glass coverslip pretreated with heptane glue, and then covered with a thin layer of halocarbon oil 700/27 (1:2; Sigma-Aldrich). The coverslip was placed on a microscope slide platform and embryos were visualized using a standard 18 upright microscope equipped with a 10× objective (Carl Zeiss). Microinjection was performed with a microinjector (model 5242; Eppendorf). Microinjection pipettes were pulled from borosilicate glass capillaries (1.2-mm outer diameter × 0.94-mm inner diameter; Harvard Apparatus), using a P-97 Flamming/brown puller (Sutter Instrument). Embryos were immersed in PBS and imaged at 20°C using a two-photon microscope (LSM 780 NLO; Carl Zeiss) equipped with a two-photon laser (Chameleon; Coherent, Inc.) and a 32×/NA 0.8 water immersion objective (Carl Zeiss). GFP was excited at λ = 950 nm. Images were acquired with Zen 2010 software (Carl Zeiss) and processed using ImageJ software (National Institutes of Health).

Immunofluorescence microscopy

Embryos were fixed in 4% paraformaldehyde (Electron Microscopy Sciences) and heptane (Merck) and stained with rabbit anti-GFP antibody (Torrey Pines) at the concentration of 1:500 and rat anti-Bnk at the concentration of 1:200. Alexa Fluor 488 anti–rabbit and Alexa Fluor 647 anti–rat (Molecular Probes) were used as secondary antibodies. HeLa and S2 cells were fixed in 4% paraformaldehyde (Electron Microscopy Sciences) in PBS for 15 min at room temperature and permeabilized with 0.1% Triton X-100 in PBS for 5 min. Samples were further incubated with an anti–rabbit myosin antibody (1:60; Biomedical Technologies, Inc.) in PBS containing 10% fetal bovine serum for 1 h at room temperature. Alexa Fluor 488– and Alexa Fluor 647–conjugated secondary antibodies (Molecular Probes) were combined with phalloidin 647 and phalloidin 488 (Molecular Probes), respectively. Fixed samples were imaged using a confocal microscope (LSM 780; Carl Zeiss) equipped with a Plan Apochromat 63×/NA 1.2 water immersion objective (Carl Zeiss). For every z-stack, each plane was separated by 0.5 µm.

Cell culture, transfection, and drug treatment

Hela cells were cultured in DMEM (Gibco) containing 10% fetal bovine serum (PAA) and 2 mM L-glutamine (Gibco) at 37°C and 5% CO_2. S2 cells stably expressing pMT-Gal4 were cultured in Express Five SFM (Gibco) containing 2 mM L-glutamine (Gibco) and puromycin (concentration 10 µg/ml; Invitrogen) at 25°C. 24 h before fixing, cells were induced with Copper(II) sulfate pentahydrate (Sigma-Aldrich) at the concentration of 700 µM.

Transfection of plasmids was performed using Fugene HD (Roche) according to the manufacturer's protocol. Hela cells were treated with either 500 nM cytochalasin D or latrunculin A for 15 min at 37°C. S2 cells were treated with 100 nm rapamycin for 20 min at 25°C.

FRAP experiments

FRAP experiments were performed using a microscope (LSM 780 NLO; Carl Zeiss) equipped with a Chameleon two-photon laser (λ = 950 nm; Coherent, Inc.). After three pre-bleaching scans, photobleaching was achieved using 50% laser power and 70 iterations. Fluorescence recovery was monitored by time-lapse imaging with 230-ms time resolution. The fluorescence intensity (FI) at each time point was divided by the average FI of the pre-bleaching images to obtain the recovery fraction. The statistical analysis was performed using a Student's *t* test.

Bottleneck siRNA

Two different siRNA were designed against Bnk: bnk1, 5′-AUGUCCAAGCGAAAUAAUGUUUU-3′ and 3′-CAUUAUUUCGCUUGGACAUUUUU-5′; bnk2, 5′-CACCUUUGAGUCGGGUUUCUU-3′ and 3′-GAAACCCGACUCAAAGGUGUU-5′. 5 µM of each construct was mixed and injected in embryos before cycle 10 when the protein starts to be expressed. A siRNA against lacZ (5′-AACCCUGGCGUUACACAACUU-3′, 5′-GUUGUGUAACGCCAGGGUUUU-3′) was injected at the concentration of 10 µM using the same protocol.

PIP strips binding assays

Bottleneck and GFP were in vitro transcribed and translated using the TNT T7 Quick-Coupled Transcription/Translation System (Promega) and labeled using 10 µCi/µl ^{35}S-methionine. ^{35}S-radiolabeled Bottleneck or ^{35}S-radiolabeled GFP were incubated with PIP strip membranes (Molecular Probes) according to the manufacturer's protocol. After extensive washes, membranes were dried and exposed on an x-ray film (Kodak) at room temperature.

Liposome flotation assay

18:1 (Δ9-Cis) PC (DOPC) 1,2-dioleoyl-*sn*-glycero-3-phosphocholine (Avanti Polar Lipids, Inc.) alone or together with each of the individual phosphoinositides (Avanti Polar Lipids, Inc.) was dissolved in a mixture of $CHCl_3$/methanol/H_2O (20:9:1) in glass vials and dried into thin films using an argon flow. Any residual trace of solvent was further dried under vacuum for at least 30 min. Liposomes were made by rehydrating the lipid films in rehydration buffer (10 mM Hepes, pH 7.4, and 150 mM NaCl) to a total lipid concentration of 3.8 mM at 62°C for 1 h and filtered through a nuclepore track-etched membrane (Waters) using a mini-extruder (Avanti Polar Lipids, Inc.) to the size of 100 nm. The final concentration of lipids in mol percentage was: 95% DOPC, 5% phospoinositides. 20 µl of the so-obtained liposomes were mixed with 40 µg of Hela cell extract expressing Bnk::GFP in Hepes buffer (10 mM Hepes, pH 7.4, and 150 mM NaCl) and incubated for 20 min at room temperature. This mixture was then adjusted to 1 M sucrose, transferred to an ultracentrifuge tube, and overlaid with 100 µl of 0.75 M sucrose in Hepes buffer, followed by 20 µl of Hepes buffer. Liposomes were centrifuged for 30 min at 60,000 rpm in a rotor (TLA100; Beckman Coulter). Protein bound to liposomes (bound fraction) were collected by removing 80 µl from the top layer of the gradient and separated by SDS-PAGE. Western blot was performed using a rabbit anti-GFP antibody (Torrey Pines) and anti–rabbit HRP (Jackson ImmunoResearch Laboratories, Inc.).

Online supplemental material

Fig. S1 shows that the PI(4,5)P_2-induced phenotype is manifested only after the onset of cellularization. Fig. S2 shows that rapamycin-dependent translocation of 5Ptase causes loss of PLCδ1-PH-GFP from the plasma membrane in S2 *Drosophila* cells. Fig. S3 shows that PI3-kinase inhibition results in reduced PI(3,4,5)P_3 levels at the plasma membrane during cellularization. Fig. S4 shows that PI(3,4,5)P_3/AM injection causes increased Bottleneck recruitment at the furrows. Fig. S5 shows that in Bottleneck-overexpressing cells, stress fibers are latrunculin A resistant. Video 1 shows Sqh::GFP dynamics in a control-injected embryo over the course of cellularization. Video 2 illustrates Sqh::GFP dynamics in a PI(4,5)P_2/AM-injected embryo over the course of cellularization. Video 3 shows Sqh::GFP dynamics in a PI(3,4,5)P_3/AM-injected embryo over the course of cellularization. Video 4 illustrates a Z-stack projection of myosin-II over the course of cellularization. Video 5 shows FRAP of a control-injected embryo expressing Sqh::GFP during the slow phase of cellularization. Video 6 shows FRAP of a control-injected embryo expressing Sqh::GFP during the fast phase of cellularization. Video 7 shows FRAP of a PI(4,5)P_2/AM injected embryo expressing Sqh::GFP during the slow phase of cellularization. Video 8 shows FRAP of a *bottleneck* mutant embryo expressing Sqh::GFP during the slow phase of cellularization. Video 9 shows FRAP in a control-injected embryo expressing YFP::Bnk during the slow phase of cellularization. Video 10 shows FRAP in a wortmannin-injected embryo expressing YFP::Bnk during the slow phase of cellularization. Online supplemental material is available at http://www.jcb.org/cgi/content/full/jcb.201309079/DC1.

We thank all members of the De Renzis laboratory and Vibor Laketa for helpful discussion. We thank K. Maeda and A.C. Gavin for valuable advice on liposome flotation assay protocols. We thank P. Fabrowski for drawing the model presented in Fig. 9. We thank D. Gilmour, A. Necakov, and J. Rink for critical reading of the manuscript. We thank the advanced light microscopy, the proteomics and protein expression core facilities (EMBL, Heidelberg, Germany), for their advice and assistance. We thank the Bloomington Drosophila Stock Center and the Drosophila Genomics Resource Center for providing fly stocks and cDNAs. We thank A. Martin and M. Leptin for providing fly stocks.

This work was supported by a Human Frontier Science Program Career Development Award (CDA) to Stefano De Renzis.

The authors declare no competing financial interests.

Submitted: 16 September 2013
Accepted: 4 April 2014

References

Apodaca, G. 2002. Modulation of membrane traffic by mechanical stimuli. *Am. J. Physiol. Renal Physiol.* 282:F179–F190.

Arrieumerlou, C., and T. Meyer. 2005. A local coupling model and compass parameter for eukaryotic chemotaxis. *Dev. Cell.* 8:215–227. http://dx.doi.org/10.1016/j.devcel.2004.12.007

Balla, T. 2013. Phosphoinositides: tiny lipids with giant impact on cell regulation. *Physiol. Rev.* 93:1019–1137. http://dx.doi.org/10.1152/physrev.00028.2012

Behrndt, M., G. Salbreux, P. Campinho, R. Hauschild, F. Oswald, J. Roensch, S.W. Grill, and C.P. Heisenberg. 2012. Forces driving epithelial spreading in zebrafish gastrulation. *Science*. 338:257–260. http://dx.doi.org/10.1126/science.1224143

Boulant, S., C. Kural, J.C. Zeeh, F. Ubelmann, and T. Kirchhausen. 2011. Actin dynamics counteract membrane tension during clathrin-mediated endocytosis. *Nat. Cell Biol.* 13:1124–1131. http://dx.doi.org/10.1038/ncb2307

Comer, F.I., and C.A. Parent. 2007. Phosphoinositides specify polarity during epithelial organ development. *Cell*. 128:239–240. http://dx.doi.org/10.1016/j.cell.2007.01.010

Fabrowski, P., A.S. Necakov, S. Mumbauer, E. Loeser, A. Reversi, S. Streichan, J.A. Briggs, and S. De Renzis. 2013. Tubular endocytosis drives remodelling of the apical surface during epithelial morphogenesis in *Drosophila*. *Nat Commun*. 4:2244. http://dx.doi.org/10.1038/ncomms3244

Fernandez-Gonzalez, R., S.M. Simoes, J.C. Röper, S. Eaton, and J.A. Zallen. 2009. Myosin II dynamics are regulated by tension in intercalating cells. *Dev. Cell*. 17:736–743. http://dx.doi.org/10.1016/j.devcel.2009.09.003

Field, S.J., N. Madson, M.L. Kerr, K.A. Galbraith, C.E. Kennedy, M. Tahiliani, A. Wilkins, and L.C. Cantley. 2005. PtdIns(4,5)P2 functions at the cleavage furrow during cytokinesis. *Curr. Biol.* 15:1407–1412. http://dx.doi.org/10.1016/j.cub.2005.06.059

Figard, L., H. Xu, H.G. Garcia, I. Golding, and A.M. Sokac. 2013. The plasma membrane flattens out to fuel cell-surface growth during *Drosophila* cellularization. *Dev. Cell*. 27:648–655. http://dx.doi.org/10.1016/j.devcel.2013.11.006

Gassama-Diagne, A., W. Yu, M. ter Beest, F. Martin-Belmonte, A. Kierbel, J. Engel, and K. Mostov. 2006. Phosphatidylinositol-3,4,5-trisphosphate regulates the formation of the basolateral plasma membrane in epithelial cells. *Nat. Cell Biol.* 8:963–970. http://dx.doi.org/10.1038/ncb1461

Gauthier, N.C., M.A. Fardin, P. Roca-Cusachs, and M.P. Sheetz. 2011. Temporary increase in plasma membrane tension coordinates the activation of exocytosis and contraction during cell spreading. *Proc. Natl. Acad. Sci. USA*. 108:14467–14472. http://dx.doi.org/10.1073/pnas.1105845108

Glotzer, M. 2005. The molecular requirements for cytokinesis. *Science*. 307:1735–1739. http://dx.doi.org/10.1126/science.1096896

Insall, R.H., and O.D. Weiner. 2001. PIP3, PIP2, and cell movement—similar messages, different meanings? *Dev. Cell*. 1:743–747. http://dx.doi.org/10.1016/S1534-5807(01)00086-7

Janetopoulos, C., and P. Devreotes. 2006. Phosphoinositide signaling plays a key role in cytokinesis. *J. Cell Biol.* 174:485–490. http://dx.doi.org/10.1083/jcb.200603156

Laketa, V., S. Zarbakhsh, E. Morbier, D. Subramanian, C. Dinkel, J. Brumbaugh, P. Zimmermann, R. Pepperkok, and C. Schultz. 2009. Membrane-permeant phosphoinositide derivatives as modulators of growth factor signaling and neurite outgrowth. *Chem. Biol.* 16:1190–1196. http://dx.doi.org/10.1016/j.chembiol.2009.10.005

Lecuit, T., and F. Pilot. 2003. Developmental control of cell morphogenesis: a focus on membrane growth. *Nat. Cell Biol.* 5:103–108. http://dx.doi.org/10.1038/ncb0203-103

Lecuit, T., and E. Wieschaus. 2000. Polarized insertion of new membrane from a cytoplasmic reservoir during cleavage of the *Drosophila* embryo. *J. Cell Biol.* 150:849–860. http://dx.doi.org/10.1083/jcb.150.4.849

Lee, D.M., and T.J. Harris. 2013. An Arf-GEF regulates antagonism between endocytosis and the cytoskeleton for *Drosophila* blastoderm development. *Curr. Biol.* 23:2110–2120. http://dx.doi.org/10.1016/j.cub.2013.08.058

Levayer, R., and T. Lecuit. 2012. Biomechanical regulation of contractility: spatial control and dynamics. *Trends Cell Biol.* 22:61–81. http://dx.doi.org/10.1016/j.tcb.2011.10.001

Martin, A.C., M. Kaschube, and E.F. Wieschaus. 2009. Pulsed contractions of an actin-myosin network drive apical constriction. *Nature*. 457:495–499. http://dx.doi.org/10.1038/nature07522

Martin-Belmonte, F., A. Gassama, A. Datta, W. Yu, U. Rescher, V. Gerke, and K. Mostov. 2007. PTEN-mediated apical segregation of phosphoinositides controls epithelial morphogenesis through Cdc42. *Cell*. 128:383–397. http://dx.doi.org/10.1016/j.cell.2006.11.051

Mason, F.M., M. Tworoger, and A.C. Martin. 2013. Apical domain polarization localizes actin-myosin activity to drive ratchet-like apical constriction. *Nat. Cell Biol.* 15:926–936. http://dx.doi.org/10.1038/ncb2796

Mayer, B.J., R. Ren, K.L. Clark, and D. Baltimore. 1993. A putative modular domain present in diverse signaling proteins. *Cell*. 73:629–630. http://dx.doi.org/10.1016/0092-8674(93)90244-K

McLaughlin, S., J. Wang, A. Gambhir, and D. Murray. 2002. PIP(2) and proteins: interactions, organization, and information flow. *Annu. Rev. Biophys. Biomol.Struct.*31:151–175.http://dx.doi.org/10.1146/annurev.biophys.31.082901.134259

Merrill, P.T., D. Sweeton, and E. Wieschaus. 1988. Requirements for autosomal gene activity during precellular stages of *Drosophila melanogaster*. *Development*. 104:495–509.

Morin, X., R. Daneman, M. Zavortink, and W. Chia. 2001. A protein trap strategy to detect GFP-tagged proteins expressed from their endogenous loci in *Drosophila*. *Proc. Natl. Acad. Sci. USA*. 98:15050–15055. http://dx.doi.org/10.1073/pnas.261408198

Moss, S.E. 2012. How actin gets the PIP. *Sci. Signal.* 5:pe7. http://dx.doi.org/10.1126/scisignal.2002839

Muthuswamy, S.K., M. Gilman, and J.S. Brugge. 1999. Controlled dimerization of ErbB receptors provides evidence for differential signaling by homo- and heterodimers. *Mol. Cell. Biol.* 19:6845–6857.

Pelissier, A., J.P. Chauvin, and T. Lecuit. 2003. Trafficking through Rab11 endosomes is required for cellularization during *Drosophila* embryogenesis. *Curr. Biol.* 13:1848–1857. http://dx.doi.org/10.1016/j.cub.2003.10.023

Pinal, N., D.C. Goberdhan, L. Collinson, Y. Fujita, I.M. Cox, C. Wilson, and F. Pichaud. 2006. Regulated and polarized PtdIns(3,4,5)P3 accumulation is essential for apical membrane morphogenesis in photoreceptor epithelial cells. *Curr. Biol.* 16:140–149. http://dx.doi.org/10.1016/j.cub.2005.11.068

Pollard, T.D. 2010. Mechanics of cytokinesis in eukaryotes. *Curr. Opin. Cell Biol.* 22:50–56. http://dx.doi.org/10.1016/j.ceb.2009.11.010

Putyrski, M., and C. Schultz. 2012. Protein translocation as a tool: The current rapamycin story. *FEBS Lett.* 586:2097–2105. http://dx.doi.org/10.1016/j.febslet.2012.04.061

Rauzi, M., P.F. Lenne, and T. Lecuit. 2010. Planar polarized actomyosin contractile flows control epithelial junction remodelling. *Nature*. 468:1110–1114. http://dx.doi.org/10.1038/nature09566

Riedl, J., A.H. Crevenna, K. Kessenbrock, J.H. Yu, D. Neukirchen, M. Bista, F. Bradke, D. Jenne, T.A. Holak, Z. Werb, et al. 2008. Lifeact: a versatile marker to visualize F-actin. *Nat. Methods*. 5:605–607. http://dx.doi.org/10.1038/nmeth.1220

Royou, A., C. Field, J.C. Sisson, W. Sullivan, and R. Karess. 2004. Reassessing the role and dynamics of nonmuscle myosin II during furrow formation in early *Drosophila* embryos. *Mol. Biol. Cell*. 15:838–850. http://dx.doi.org/10.1091/mbc.E03-06-0440

Salbreux, G., G. Charras, and E. Paluch. 2012. Actin cortex mechanics and cellular morphogenesis. *Trends Cell Biol.* 22:536–545. http://dx.doi.org/10.1016/j.tcb.2012.07.001

Schejter, E.D., and E. Wieschaus. 1993a. bottleneck acts as a regulator of the microfilament network governing cellularization of the *Drosophila* embryo. *Cell*. 75:373–385. http://dx.doi.org/10.1016/0092-8674(93)80078-S

Schejter, E.D., and E. Wieschaus. 1993b. Functional elements of the cytoskeleton in the early *Drosophila* embryo. *Annu. Rev. Cell Biol.* 9:67–99. http://dx.doi.org/10.1146/annurev.cb.09.110193.000435

Schultz, C. 2003. Prodrugs of biologically active phosphate esters. *Bioorg. Med. Chem.* 11:885–898. http://dx.doi.org/10.1016/S0968-0896(02)00552-7

Schultz, C. 2010. Challenges in studying phospholipid signaling. *Nat. Chem. Biol.* 6:473–475. http://dx.doi.org/10.1038/nchembio.389

Schweisguth, F., J.A. Lepesant, and A. Vincent. 1990. The serendipity alpha gene encodes a membrane-associated protein required for the cellularization of the *Drosophila* embryo. *Genes Dev.* 4:922–931. http://dx.doi.org/10.1101/gad.4.6.922

Simpson, L., and E. Wieschaus. 1990. Zygotic activity of the nullo locus is required to stabilize the actin-myosin network during cellularization in *Drosophila*. *Development*. 110:851–863.

Sisson, J.C., C. Field, R. Ventura, A. Royou, and W. Sullivan. 2000. Lava lamp, a novel peripheral golgi protein, is required for *Drosophila melanogaster* cellularization. *J. Cell Biol.* 151:905–918. http://dx.doi.org/10.1083/jcb.151.4.905

Sokac, A.M., and E. Wieschaus. 2008. Local actin-dependent endocytosis is zygotically controlled to initiate *Drosophila* cellularization. *Dev. Cell*. 14:775–786. http://dx.doi.org/10.1016/j.devcel.2008.02.014

Stambolic, V., A. Suzuki, J.L. de la Pompa, G.M. Brothers, C. Mirtsos, T. Sasaki, J. Ruland, J.M. Penninger, D.P. Siderovski, and T.W. Mak. 1998. Negative regulation of PKB/Akt-dependent cell survival by the tumor suppressor PTEN. *Cell*. 95:29–39. http://dx.doi.org/10.1016/S0092-8674(00)81780-8

Suh, B.C., T. Inoue, T. Meyer, and B. Hille. 2006. Rapid chemically induced changes of PtdIns(4,5)P2 gate KCNQ ion channels. *Science*. 314:1454–1457. http://dx.doi.org/10.1126/science.1131163

Sullivan, W., and W.E. Theurkauf. 1995. The cytoskeleton and morphogenesis of the early *Drosophila* embryo. *Curr. Opin. Cell Biol.* 7:18–22. http://dx.doi.org/10.1016/0955-0674(95)80040-9

Theurkauf, W.E. 1994. Actin cytoskeleton. Through the bottleneck. *Curr. Biol.* 4:76–78. http://dx.doi.org/10.1016/S0960-9822(00)00019-1

Thomas, J.H., and E. Wieschaus. 2004. src64 and tec29 are required for microfilament contraction during *Drosophila* cellularization. *Development*. 131:863–871. http://dx.doi.org/10.1242/dev.00989

Uehara, R., G. Goshima, I. Mabuchi, R.D. Vale, J.A. Spudich, and E.R. Griffis. 2010. Determinants of myosin II cortical localization during cytokinesis. *Curr. Biol.* 20:1080–1085. http://dx.doi.org/10.1016/j.cub.2010.04.058

Varnai, P., B. Thyagarajan, T. Rohacs, and T. Balla. 2006. Rapidly inducible changes in phosphatidylinositol 4,5-bisphosphate levels influence multiple regulatory functions of the lipid in intact living cells. *J. Cell Biol.* 175:377–382. http://dx.doi.org/10.1083/jcb.200607116

von Stein, W., A. Ramrath, A. Grimm, M. Müller-Borg, and A. Wodarz. 2005. Direct association of Bazooka/PAR-3 with the lipid phosphatase PTEN reveals a link between the PAR/aPKC complex and phosphoinositide signaling. *Development*. 132:1675–1686. http://dx.doi.org/10.1242/dev.01720

Wieschaus, E., and D. Sweeton. 1988. Requirements for X-linked zygotic gene activity during cellularization of early *Drosophila* embryos. *Development*. 104:483–493.

Wong, R., I. Hadjiyanni, H.C. Wei, G. Polevoy, R. McBride, K.P. Sem, and J.A. Brill. 2005. PIP2 hydrolysis and calcium release are required for cytokinesis in *Drosophila* spermatocytes. *Curr. Biol.* 15:1401–1406. http://dx.doi.org/10.1016/j.cub.2005.06.060